NeuroImage: Clinical 49 (2026) 103940

Contents lists available at ScienceDirect

NeuroImage: Clinical

journal homepage: www.elsevier.com/locate/ynicl

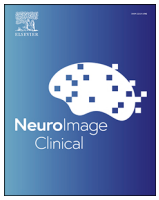

Individualized functionnectome for the statistical assessment of white matter circuits underlying task-fMRI activations in glioma patients

Giovanni Sighinolfi [a,*], Alexander Leemans [b], David Neil Manners [a,c], Elena Cantoni [a], Gianfranco Vornetti [a,d], Lorenzo Motta [a], Enrico Franceschi [a], Caterina Tonon [a,d], Raffaele Lodi [a,d,1], Alberto De Luca [b,1]

[a] IRCCS Istituto delle Scienze Neurologiche di Bologna, Bologna, Italy
[b] Image Sciences Institute, University Medical Center Utrecht, Utrecht, Netherlands
[c] Department for Life Quality Studies, University of Bologna, Bologna, Italy
[d] Department of Biomedical and Neuromotor Sciences, University of Bologna, Bologna, Italy

A B S T R A C T

The Functionnectome framework enables the projection of task-related fMRI signals onto the underlying white matter pathways, using anatomical priors derived from structural connectivity. However, the existing "standardized" priors are based on averaged tractograms from healthy controls and cannot accurately capture the altered anatomy found in patients with brain lesions.

This study extends the Functionnectome framework by generating individualized anatomical priors from subject-specific diffusion MRI tractography, allowing for improved integration of functional and structural data in patients with brain tumors. Twenty-six patients with gliomas (9 females; mean age 43 ± 17 years) underwent 3 T MRI, including a multishell diffusion protocol and task-based fMRI targeting motor and/or language functions. Whole-brain tractography was reconstructed using three methods (TensorDet, PFT, and iFOD2) and converted into voxelwise individualized priors. Functionnectome maps were estimated using both standardized and individualized priors, and Z-statistic activation maps were obtained via GLM analysis. Similarity metrics and atlas-based consistency were used to compare standardized and individualized Functionnectomes.

Functionnectomes derived from probabilistic tractography showed moderate correlations with standardized Functionnectomes (average Pearson's r ≈ 0.5), highlighting the influence of individual structural variability while maintaining comparable activation patterns. The PFT-based Functionnectome exhibited superior anatomical plausibility, with consistent overlap with expected motor white matter tracts and identification of relevant bundles in up to 100% of cases, compared to 50–60% with standardized priors.

The individualized Functionnectome enhances the anatomical validity and subject specificity of structure–function mapping, advancing precision neuroimaging for clinical and neurosurgical applications.

1. Introduction

The integration of functional and diffusion magnetic resonance imaging (fMRI, dMRI), together with the development of novel analytical approaches to fully exploit their complementary strengths, is a growing field of scientific research. dMRI enables tractography-based reconstruction of white matter pathways, yielding whole-brain tractograms that estimate structural connectivity between regions (Basser et al., 2000; Jeurissen et al., 2017). fMRI, in contrast, captures the temporal dynamics of neural activity by measuring the BOLD signal in resting-state or task-based paradigms (Chen and Glover, 2015; Logothetis, 2003). When combined, these techniques offer a richer understanding of brain organization, as their integration can reveal patterns of synchronized activity, which are supported by specific structural pathways (Park and Friston, 2013).

Different approaches have been developed over the recent years to efficiently integrate the two techniques and maximize the information extraction, with promising results (Liégeois et al., 2020; Mandke et al., 2018; Ritter et al., 2013). Most of these approaches are based on the connectomic analysis of the functional and structural connectivity (Fornito et al., 2015). These methods attempt to create frameworks for the extraction of novel biomarkers, rather than to obtain a direct link between structural connectivity and brain function. Other studies have followed this research line, aiming to statistically explore the function of white matter circuits through the combination of dMRI and resting-state (Calamante et al., 2013) or task-based (Nozais et al., 2021; Tarun et al.,

* Corresponding author at: IRCCS Istituto delle Scienze Neurologiche di Bologna Via Altura 3, Bologna 40139, Italy.
E-mail address: giovanni.sighinolfi3@unibo.it (G. Sighinolfi).
[1] These authors contributed equally.

https://doi.org/10.1016/j.nicl.2025.103940
Received 5 November 2025; Received in revised form 24 December 2025; Accepted 27 December 2025
Available online 31 December 2025

2020) fMRI. Among these, the Functionnectome (Nozais et al., 2023, 2021) proposed to project task-related fMRI on the underlying white matter connections, to investigate the functional role of specific brain circuits. It integrates dMRI and fMRI to derive maps of white matter activation, and investigate brain circuits' functional involvement during task-related cerebral processes, based on standardized priors of anatomical connectivity. The significance of the Functionnectome in investigating the brain circuitry underlying the functional activations was demonstrated by showing that plausible white matter pathways were involved in presence of motor, language and working memory tasks. In addition, the involvement of additional tracts, hypothesized based on their location, which had not been verified before in humans using classical methods, emerged using the Functionnectome; the bilateral frontal superior longitudinal tract is one example, with a role in working memory (Nozais et al., 2021; Rojkova et al., 2016).

In both the original Functionnectome framework and its updated versions (Nozais et al., 2023, 2021), the anatomical prior of structural connectivity, used to project the BOLD signal onto the white matter, is based on a template. In practice, the template has been determined once by averaging the whole-brain connectivity of a large group of healthy controls, and is then re-applied as-is to new subjects. As such, per-definition, this "standardized" anatomical priors do not account for the individual variability of the subject's brain structure. Although structural connectivity patterns are largely consistent across individuals, subject-specific differences are always present and can critically influence brain function (Alstott et al., 2009). This becomes particularly relevant in the presence of intracranial expansive lesions, which can markedly alter local anatomy. In such cases, standardized anatomical priors may fail to accurately represent the true structural connectivity between brain regions, especially in the vicinity of the lesion. Additionally, an individualized approach aiming to statistically assess the functional involvement of the patient's white matter tracts during task paradigms can be especially relevant for tumoral cases, where preserving functionally active brain regions is of paramount importance (Castellano et al., 2017; Lakhani et al., 2023).

In this study, we propose and evaluate a novel method to integrate individualized structural connectivity information into the functionnectome, aiming to reliably identify the involvement of white matter pathways underlying cortical activation in patients with intracranial brain tumors.

2. Methods

2.1. MRI data acquisition

Patients with expansive lesions of the brain who had undergone an MRI examination at the scientific institute Functional and Molecular Neuroimaging Unit, IRCCS Istituto delle Scienze Neurologiche di Bologna (Bologna, Italy) were retrospectively included from the database of the Neuroimaging Laboratory. All subjects were acquired using a Siemens MAGNETOM Skyra 3 T scanner equipped with a high-density head/neck array coil (64 channels). The MRI protocol included a high-resolution volumetric T1-weighted sequence (MPRAGE, sagittal acquisition, 1 mm isotropic voxel, FOV 256 mm, TR/TE = 2300/2.98 ms, TI = 900 ms, flip angle 9°, acquisition time 5:21 min) and a multishell dMRI protocol (2D single-shot EPI sequence, 87 slices, 2 mm isotropic voxel, no slice gap, TR/TE = 4300/98 ms, flip angle 90°, FOV 220 mm) with 114 independent volumes acquired with anterior-posterior (AP) phase encoding direction (8 at b = 0 s/mm^2, 12 at b = 300 s/mm^2, 30 at b = 1000 s/mm^2, 64 at b = 2000 s/mm^2, acquisition time 8:41 min) and 50 independent with posterior-anterior (PA) phase encoding direction (8 at b = 0 s/mm^2, 12 at b = 300 s/mm2, 30 at b = 1000 s/mm^2, acquisition time 4:04 min) (Castellaro et al., 2020; Manners et al., 2022). The patients also performed a battery of motor and/or language task-based fMRI acquisitions with auditory stimulation, chosen on the basis of tumor location, using a block design with 30 s blocks and a total acquisition time of 4:30 min (2.5 mm isotropic resolution, TR/TE = 735/37 ms, FOV = 235 mm, flip angle = 53°). The paradigms are described in the Supplementary Material Part 1. The fMRI protocol also included a shorter sequence, referred to as "reference scan" in the following, with only 2 volumes and the same acquisition parameters, except for the TR = 5760 ms, used to achieve better contrast between tissues and improve registration with structural images.

A subsample of 10 patients was randomly chosen for initial validation of the results.

The study protocol was designed in accordance with the observance of the Code of Ethics of the World Medical Association (Declaration of Helsinki) and approved by the local Ethics Committee (CE 738–2021-SPER-AUSLBO - 21,141 − ID 2372). Written informed consent was obtained from all participants involved in the study.

2.2. MRI data preprocessing

Diffusion MRI data were preproccesed using an in-house written pipeline based on FSL (Jenkinson et al., 2012), version 6, AFNI (Cox, 1996), version 20.3.02, MRtrix3 (Tournier et al., 2019), version 3.0.2, and Scilpy, version 1.6.0 (https://github.com/scilus/scilpy.git).

Image denoising was performed with the MRtrix3 dwidenoise function (Dhollander et al., 2019, 2016), which uses a principal component analysis approach, with the default settings. Susceptibility-related distortions in the EPI acquisition were estimated from the 16 denoised b = 0 s/mm^2 images acquired with AP and PA phase-encoding directions, using the FSL topup function (Andersson et al., 2003), with the FSL predefined "b02b0.cnf" configuration settings; subsequently, a combined correction for susceptibility, eddy-current effects, and signal dropout, most commonly induced by subject movement, was performed with FSL eddy (Andersson and Sotiropoulos, 2016), based on the topup estimates. Images were skull-stripped using FSL bet with a fractional intensity threshold of 0.4. The fiber orientation distribution function (fODF) was modelled with multishell-multitissue constrained spherical deconvolution (Jeurissen et al., 2014) and estimated using both the Dhollander algorithm within MRtrix3 dwi2response/dwi2fod (Dhollander et al., 2019, 2016) with the Tournier spherical harmonics basis (order 8, all shells used) (Tournier et al., 2019) and the Scilpy scil_frf_msmt.py/scil_fodf_msmt.py algorithms with the Descoteaux spherical harmonics basis (order 8, all shells used) (Descoteaux et al., 2007), both using the default settings. Image registration to the MNI standard space was achieved via linear registration to the T1-weighted image using FSL epi_reg (Jenkinson et al., 2002), followed by a non-linear registration to the MNI performed with FSL fnirt. The quality of the registration was visually checked.

Task-based fMRI data required a minimal preprocessing, achieved using part of an in-house written pipeline (Muccioli et al., 2023) based on FSL (Jenkinson et al., 2012): fMRI data were motion-corrected using FSL mcflirt (Jenkinson et al., 2002) and skull-stripped using FSL bet; the correction of susceptibility distortion was performed by applying the warpfield estimated from AP-PA dMRI data using topup. Registration to the MNI was performed via linear registration to the fMRI reference scan, which was then linearly registered to the T1-weighted image using epi_reg, and lastly non-linearly registered to the MNI using FSL fnirt, followed by a visual check of the result. Other common steps for the preprocessing of fMR images, including spatial smoothing, are not needed in this framework, because the combination of the fMRI signal from distant yet structurally linked voxels has an analogous effect of improving the SNR, while being guided by actual brain circuits. This ensures high spatial precision and sensitivity (Nozais et al., 2021).

2.3. Functionnectomes derivation

For each available subject and task paradigm, the functionnectomes were derived using both the standardized and newly-developed individualized approaches. While the standardized approach required the

fMRI data only, as the anatomical priors were already provided, and followed the procedure for the map extraction described in (Nozais et al., 2021), the individualized one needed the definition of the method for the extraction of the individualized priors as well, which is described in Section 2.3.2.

In practice, this is achieved by projecting the fMRI timeseries associated to a specific brain voxel onto the underlying paths that connect this voxel to the rest of the brain. The paths are provided by anatomical priors, i.e. probability maps of the existence of a connection between a given voxel and any other brain voxel, which serve as weights in this framework. Once the functionnectome is extracted, the wide range of analytical approaches applicable to (task-)fMRI data is available for the novel data as well.

2.3.1. Standardized functionnectome

In the original work, the anatomical priors were estimated from the whole-brain tractograms of a normative population of 100 Human Connectome Project (HCP) (Van Essen et al., 2013) participants. In the latest update of the Functionnectome framework (Nozais et al., 2023), the tractograms were generated based on the 3 T data from the HCP, acquired using a spin-echo EPI sequence (1.25 mm isotropic voxel, b-values = 1000, 2000, 3000 s/mm^2, 90 total diffusion directions acquired per shell, 18b = 0 images). The whole-brain probabilistic tractography was performed using the combination of local and a Particle Filter Tracking (PFT) (Girard et al., 2014) within TractoFlow (Theaud et al., 2020). An algorithm described in (Nozais et al., 2023) was also adopted to extend streamlines deeper into the grey matter, ensuring a more accurate projection of the BOLD signal onto the white matter. For the extraction of the probability maps, the tractograms were then registered to the MNI standard brain. Then, for each voxel, all streamlines intersecting the selected voxel were derived from tractograms, binarised and averaged across subjects, using the "Disconnectome" function of the BCBtoolkit (Foulon et al., 2018). These "standardized" priors are publicly available as part of the Functionnectome framework on GitHub (https://github.com/NotaCS/Functionnectome).

The intensity of the functionnectome image in voxel v at time t, $Functionnectome(v,t)$, is calculated using Equation (1), where M is a brain mask and m identifies a voxel within the mask, P_m is the probability map of structural connectivity derived from voxel m, provided by the set of standardized anatomical priors, and $F(m,t)$ is the BOLD signal of voxel m at time t.

$$Functionnectome(v,t) = \sum_{m \in M} \frac{P_m(v) \times F(m,t)}{\sum_{m \in M} P_m(m)} \quad (1)$$

The output functionnectome is a 4D image, where the fMRI data at each time point are projected onto the brain to produce a new volume. In words, the value of voxel v is equal to the sum of the BOLD signal from every voxel in the brain, weighted by the probability of their connection to v, and divided by the sum of all those probabilities (Nozais et al., 2021). The derived functionnectomes were then analyzed by fitting the data to the expected variation of the BOLD signal as a function of time, using a General Linear Model (GLM) (Woolrich et al., 2001), as most commonly done for task-fMRI data. The generation of one functionnectome took about 30 min using 8 CPU cores. The statistical significance was set at Z-statistic > 3. An example of the estimated functionnectome and the resulting statistical analysis of the functionally activated areas can be seen in Supplementary Fig. S1.

2.3.2. Individualized functionnectome

This subsection is divided into two paragraphs: the first describes the methods used for whole-brain tractography, which constitute the basis for the anatomical priors; the second describes how the tractograms were converted into the individualized priors.

Whole-brain tractography.

Whole-brain tractography was performed using three different approaches:

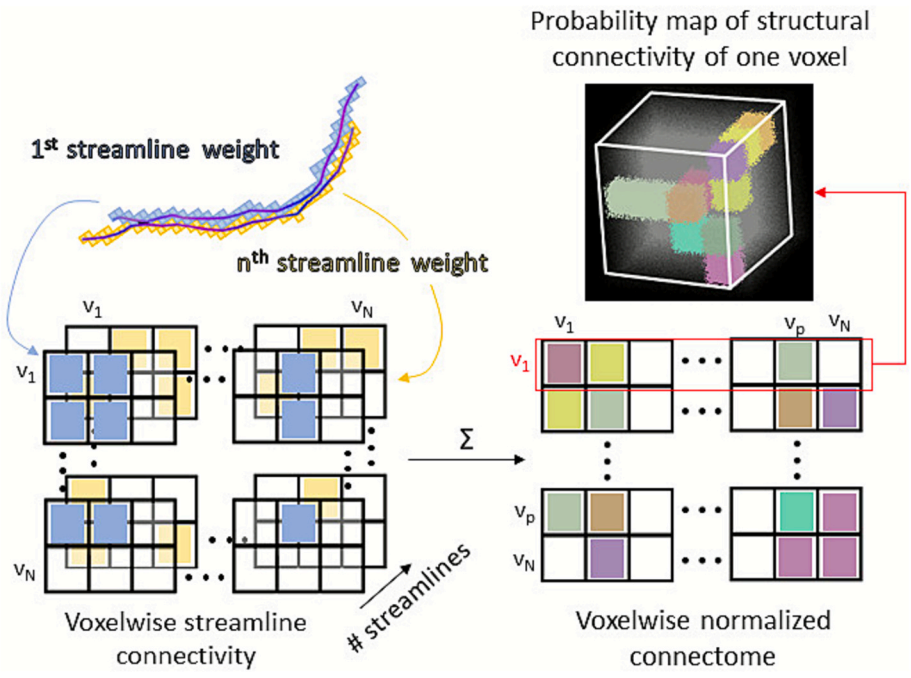

Fig. 1. Left: scheme of the conversion of the tractogram to the connectome. The representation of the connectome as a connectivity matrix is achieved by adding the weight of each streamline to those matrix elements of the voxelwise connectome that correspond to all the possible combinations of voxels that are crossed by the streamline. Right: scheme of the conversion of the connectome to the anatomical priors of structural connectivity. The output connectome obtained by summing the streamline weights element-wise in the matrix, is encoded by the different color in each cell. The matrix element corresponds to the probability of the connectivity between any two given voxels, and each row describes the connectivity of a specific voxel with every other. Since there is a unique correspondence between the matrix element and corresponding position in the MNI space, the rows can then be reshaped to the 3D space, to represent the probability of the connectivity of any voxel with every other in the MNI space.

1. PFT. Particle Filter Tracking (PFT) (Girard et al., 2014) is a local probabilistic tractography method, which estimates the distribution of potential streamlines using probabilistic samples and weighs them using anatomical information provided by an underlying tissue segmentation. The PFT tractography was combined with a classical local algorithm tractography. This approach was chosen to reproduce the same method used to construct the standardized anatomical prior in the update to the original Functionnectome paper (Nozais et al., 2023), and based on Scilpy-derived fODF. To reproduce the work by Nozais and colleagues, the parameters used to perform the tractography were set analogously: the shape factor for the elongated symmetric diffusion tensor of the fiber response function was $1.5 \times 10 - 3$ mm^2/s; step-size was 0.5 mm; maximal angle between steps was 20°; otherwise default parameters. The seeding was done on the whole white matter segmented using FSL fast (Zhang et al., 2001) (initially run on the T1-weighted image), with 10 seeds per voxel for the PFT and 5 seeds per voxel for the local tracking. The two tractograms were combined preserving unique streamlines only.
2. iFOD2. Improved probabilistic streamlines tractography by 2nd order integration over fibre orientation distributions (iFOD2) (Tournier et al., 2010) is a local probabilistic tractography method, that samples streamline directions from the FOD at each point. By using a second-order integration scheme, it accounts for local fibre orientation uncertainty while reducing directional bias, producing streamlines whose distribution reflects the probability of underlying white matter pathways. This approach was chosen since iFOD2, implemented in MRtrix3 is one of the most widely selected tractography approaches in the diffusion community. The anatomically constrained tractography (ACT) framework (Smith et al., 2012) was adopted: a 4D'5-tissue-type' image was generated from the FreeSurfer segmentation of the brain from the T1-weighted image, using MRtrix3 5ttgen; then, the interface between grey (including the subcortical nuclei, amygdalae and hippocampi) and white matter was generated with MRtrix3 5tt2gmwmi and was used for streamline seeding, imposing the anatomically-informed streamline selection provided by ACT, a minimum streamline length of 30 mm and allowing backtracking. The other parameters were set to the default values: step-size was 1 mm, maximal angle between steps was 45°, FOD amplitude cutoff value was 0.05; re-tracking of streamlines was allowed, and up to 1 million streamlines were selected.
3. TensorDet. TensorDet is a tensor-based, deterministic algorithm (Basser et al., 2000), which, at each streamline step, fits the diffusion tensor to the local trilinearly-interpolated diffusion data, and determines the streamline trajectory as the principal eigenvector of that tensor. A traditional tensor-based tractography approach, which is computationally less-requiring than CSD-based ones, was chosen for comparison to the CSD-based probabilistic methods. To apply this approach, the preprocessed diffusion images were directly provided to the algorithm and the 4th-order Runge-Kutta integration was used, seeding from the grey-white matter interface as in the iFOD2 case. Also in this case, the tractography was performed within the MRtrix3 framework.

No exclusion masks were used for any of the tractography methods, so that crossing tumor tissue was allowed. The tractograms were then registered to the MNI standard brain using the combination of linear and non-linear transformations previously derived. The MNI brain mask was then used to truncate streamlines going outside of the brain and into the CSF, and a minimum streamline length of 30 mm was imposed again. The final output tractograms in the MNI space were formed by about 1 million streamlines for each type of tractogram. Examples of whole-brain tractograms generated with the three approaches for a single case are shown in Supplementary Fig. S2.

Lastly, the Spherical-deconvolution Informed Filtering of Tractograms (SIFT2) (Smith et al., 2015) was applied to both the CSD-based tractograms (i.e., iFOD2 and PFT). It determines an appropriate cross-sectional area multiplier for each streamline, so that a weight representing the streamline "plausibility" could be assigned. In the case of TensorDet, a unitary weight was assigned to each streamline, since SIFT2 could not be applied to a tensor-based algorithm.

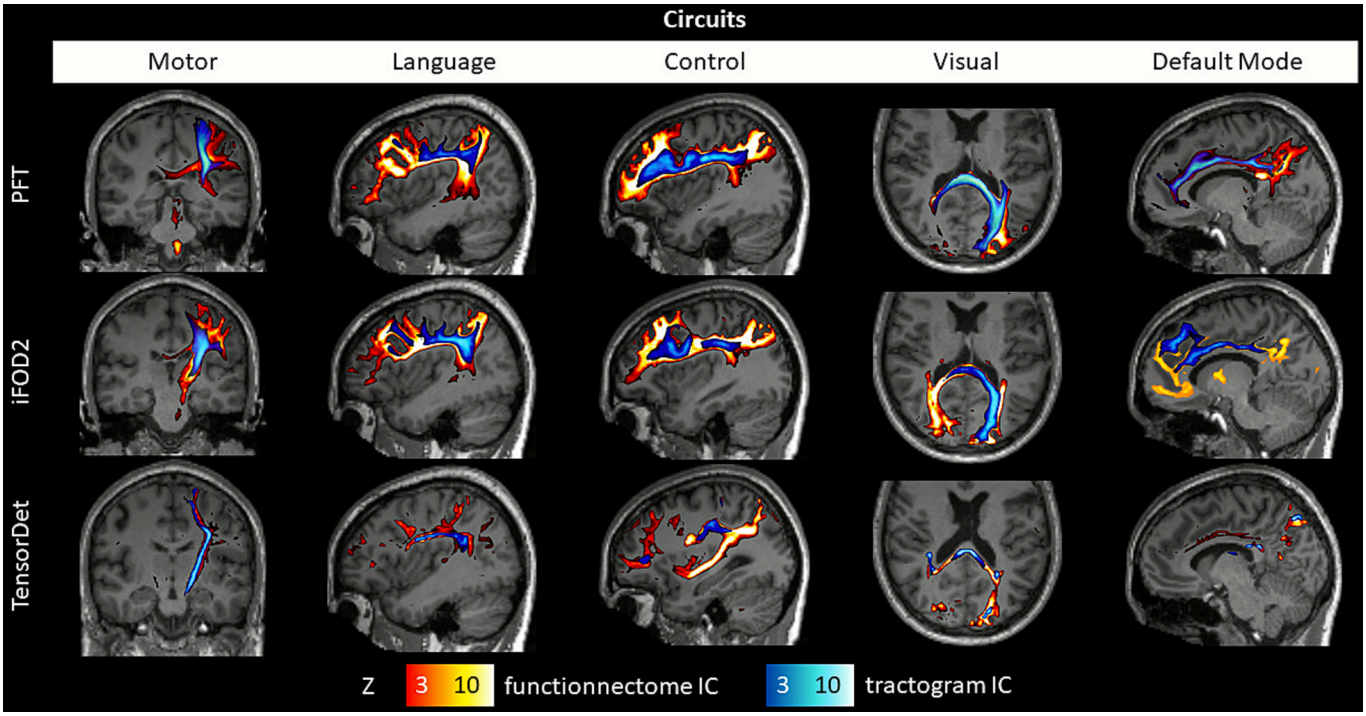

Fig. 2. Example of correspondence between tractogram and functionnectome independent components for the main brain circuits. The slice displayed was the one with the highest spatial overlap between functionnectome and tractogram components. Visually, the similarity between tractogram and functionnectome is significantly higher for the probabilistic approaches compared to the deterministic one.

Tractogram to anatomical priors conversion

To optimize the conversion of the individual subject's tractogram to the individualized anatomical priors, the process was divided in two steps: firstly, the tractogram was converted to a voxel × voxel connectome, then the latter was transformed to the set of subject-specific anatomical priors.

Conversion tractogram to connectome. The conversion of the tractogram to a voxel-wise structural connectome (about 200000 × 200000 matrix in the 2 mm MNI space) was performed with an in-house written Python 3.12 code, mostly based on NumPy 2.0 (Harris et al., 2020) and NiBabel 5.1 (Brett et al., 2023). First, a unique identifier was assigned to each of the 91 × 109 × 91 voxels in the MNI space, then cropped to the N voxels within the brain mask, obtained as the sum of the grey and white matter segmentations provided by the 5-tissue-type analysis. Then, a N × N matrix was created, ensuring, through the previous step, that there is a one-to-one correspondence between the voxel location in the MNI space and the row/column of the matrix, via the unique identifier. For each streamline, the crossed voxels were extracted, and the streamline weight provided by SIFT2 was added to the matrix elements corresponding to all the possible pairs of the selected voxels. This procedure is illustrated in Fig. 1 (left side). Repeating the same process for each streamline, the final connectome was obtained. As a last step, the values were normalized in the [0,1] range. This process takes about 1:30–2 h for about 1 million streamlines, using 8 CPU cores, and about 30 GB of RAM.

Conversion connectome to anatomical priors. Once the final connectome was generated, each row (or column) of the matrix corresponded to all the possible structural connections that the voxel associated to the selected row had with every other voxel in the brain, and the matrix element corresponded to the probability of the connection between the two selected voxels, mediated by the sum of the weights of all the streamlines that connected those two voxels. Given the one-to-one correspondence between the matrix rows/columns and the voxel coordinates, each row could be reshaped to build the intensity levels in the 91 × 109 × 91 MNI standard space, so that the 3D probability map of the connectivity of the selected voxel with every other, i.e., the anatomical prior, is obtained. Repeating this process for every row of the matrix, we obtain one anatomical prior of structural connectivity for each brain voxel, as in the original work. A schematic representation of this procedure is depicted in Fig. 1 (right side). The resulting set of ~ 200000 3D maps were stored into a single hierarchical data format (h5) file (https://www.h5py.org/) to save disk space and maintain conformity with the data structure of the original work. To reduce the computational time, the conversion of rows to the 3D maps was simultaneously performed for chunks of 2000 rows: each chunk was converted to a separate h5 file, then merged into a single one. The entire process takes about 2 h on 8 CPU cores for 200,000 voxels and the output file takes about 3 GB on disk.

Lastly, the calculation of the functionnectomes and the following statistical analysis were performed using the same procedure described in Section 2.3.1, but adopting the newly-derived, individualized priors. This was possible since the data structure of the anatomical priors was preserved equal to the one of the standardized case.

2.4. Experiments

In absence of a ground truth to compare the individualized Functionnectome with, we set up three experiments to evaluate the reliability of the proposed approach, and compare it to the original one, which are described in the three paragraphs of this subsection. The first was to evaluate the reliability of the individualized priors, by correlating corresponding independent components of the functionnectome and the tractogram; the second was to evaluate the similarity between the individualized and standardized functionnectome activation maps; the third was to assess how consistently the plausible tracts underlying activations were identified by the individualized and standardized functionnectomes for each functional paradigm.

2.4.1. Reliability of the priors

The reliability of the priors was evaluated on a subsample of 10 random patients, following a method similar to the one used in the original work (Nozais et al., 2021), which was adapted from O'Muircheartaigh's and Jbabdi's work (O'Muircheartaigh and Jbabdi, 2018). It consists of calculating Pearson's correlation between corresponding independent components (ICs) of functional MRI data on one side and structural connectome on the other side. Although this is not a validation in the strict sense, as there is no ground truth to compare the anatomical priors with, this indeed measures their reliability, and it was used for this purpose in the original Functionnectome work as well (Nozais et al., 2021). The method described by O'Muircheartaigh and Jbabdi was reproduced step-by-step, with the only exception that the functional data used to extract the independent components were those of the functionnectome itself, not the resting-state fMRI, as this sequence was not available for all subjects. While task-based fMRI data could be used, preliminary analyses demonstrated that the ICs were less clearly defined than when using rs-fMRI (except for the network directly involved by the task itself), potentially confounding our main goal of evaluating the impact of anatomical priors. Thus, we decided to use the functionnectomes, acknowledging that we would have had stronger correlations compared to the original work, as the functionnectome ICs were mainly localized in the white matter as well, by definition.

O'Muircheartaigh's and Jbabdi's procedure was implemented in a self-written Python 3.12 code based mainly on scikit-learn 1.4 (https://scikit-learn.org/dev/index.html), including the following steps:

- For each subject separately and using the same approach described in section 2.3.2, the tractogram was converted to a (grey matter voxels) × (all brain voxels) connectivity matrix, as the aim is to separate white matter bundles by clustering paired grey matter'nodes' and white matter'edges'. The connectome was then normalized to have mean equal to 0 and standard deviation equal to 1.
- The columns, i.e., the whole brain targets, were shuffled, and 10,000 columns were iteratively selected. A principal component analysis (PCA) was used to reduce the number of variables to 4000; then 10,000 more columns were added to the 4000 retrieved previously and all-together reduced again to 4000, until all columns were considered. This dimensionality reduction was needed because ICA should not be run with a higher number of variables (the columns, whole-brain targets), compared to observables (the rows, grey matter voxels), otherwise the mixing matrix estimate becomes ill-conditioned and the decomposition matrix unstable.
- An ICA was applied to the PCA-reduced space to extract 30 spatial independent components. The components were then projected back to the original space for the visualization and the subsequent analysis.
- The ICA was also performed on the 4D functionnectome using FSL melodic to also extract 30 independent components.
- Pearson's correlation between each tractogram and functionnectome independent component was calculated. The main tracts traditionally considered associated with motor function (cortico-spinal tract), language function (arcuate fasciculus), control function (superior longitudinal fasciculus), visual function (optic radiations) and default mode network (cingulum bundle), were visually identified among the functionnectome components. The tractogram component corresponding to the functionnectome component for those circuits was identified as the one with the highest correlation and underwent visual verification. We then compared the Pearson's

correlation obtained using the different tractography approaches, to establish whether one approach produced significantly more reliable results compared to the others. Approaches not passing this validation would be discarded for the following step.

2.4.2. Similarity metrics between functionnectomes

The similarity between each individualized and the standardized functionnectome was quantified as a metric to test the reliability of the individualized outcomes, compared to the standardized results. Note that we did not expect full accord between them, as the uniqueness of the single-subject connectivity is the core aspect of using an individualized approach. However, a certain degree of similarity was expected, since every subject shares analogous structural connectivity patterns. After having extracted the activation maps at $Z > 3$, the Pearson's correlation was calculated between the Z-statistic maps at the intersected voxels, while the Dice coefficient was estimated between the entire binarized masks. The rationale of using the Dice coefficient in addition to the Pearson's correlation was to evaluate the agreement between outputs, not only in terms of the distribution of the statistical significance of the activations, but also of the spatial overlap of the maps. In addition, the percentage overlap of the thresholded Z-statistic maps with a manually-drawn segmentation of the tumor was measured. Group-level comparison of the similarity metrics between the different approaches was conducted separately for motor and language tasks. Metrics were computed on the subsample of 10 patients, with the goal of identifying the most effective individualized method relative to the standardized case, and ultimately selecting one to advance to the final step of the analysis.

2.4.3. Functionnectome overlap with tract atlas

The final step was to evaluate the plausibility and consistency of the white matter pathways derived with both individualized and standardized functionnectomes as compared to an anatomically driven dissection of white matter pathways (Radwan et al., 2022). For this step, all 26 available patients were considered. The template tracts were provided in the.tck format and converted to NIfTI using MRtrix3, in order to compare them with the Z-statistic images of the functionnectome. For each subject, we measured the percentage overlap between the functionnectome and each of the 68 template tracts, and extracted the five tracts with the highest overlap. Then, for each tract, we calculated the proportion of subjects in which it appeared among the top five, using this value as an estimate of across-subject reproducibility. The overlap of the individualized and the standardized functionnectomes with the atlas tract was calculated for each task separately, thresholding the activation maps at $Z > 3$, $Z > 4$ and $Z > 7$. A qualitative inspection was conducted to assess the plausibility of the paths identified by the functionnectome, based on the template tracts that they overlapped most.

2.5. Statistical analysis

Statistical analyses were conducted using self-written R 4.2.3 codes, based on rstatix 0.7.2.

A Shapiro-Wilk test was run to check the normality of data distribution before the statistical comparison. Based on the result, a *t*-test or a Mann-Whitney *U* test was run to compare: the Pearson's correlation between functionnectome and tractogram independent components across the three tractography approaches; the Pearson's correlation and the Dice coefficient between the standardized and the individualized functionnectomes.

Statistical significance was set at $p < 0.05$ after correction for multiple comparisons using the false discovery rate method.

3. Results

3.1. MRI acquisition

Twenty-six patients (9 females, age: 43 ± 17 years) with brain gliomas were included. Sixteen tumors were classified as glioblastoma IDH-wildtype, 7 as astrocytoma (5 IDH-mutant grade II, 1 IDH-mutant grade III, 1 pilocytic) and 3 as glioneuronal. Thirteen gliomas were located in the left hemisphere (among which 8 in the frontal, 3 in the temporal, and 2 in the parietal lobe), twelve in the right hemisphere (4 frontal, 2 fronto-temporal, 1 fronto-parietal, 2 parietal, 1 hippocampal), and one was median (parieto-occipital).

A total of thirty-one language tasks (20 phonemic fluency, 11 semantic fluency) and 45 motor tasks (13 bilateral finger tapping, 5 bilateral foot plantar flexion and 9 lip protrusion) were available across subjects. Sup. Table S1 summarizes these results, by grouping the location of the tumor and the fMRI tasks performed for each tumor classification.

3.2. Tractogram to anatomical priors conversion

An example of the anatomical prior derived for a single voxel using the three individualized approaches, compared to the standardized one, is shown in Supplementary Fig. S3. In general, we observed that all the individualized methods were successful in providing the desired specificity of the individualized connectivity for the subject under study. They typically corresponded to a subgroup of all the connections found across 100 subjects and accounted for in the standardized priors, and they were usually associated to a specific family of fibers among association, projection and commissural. As a result, the standardized priors extended to larger portions of the brain, typically spanning different lobes, while the individualized ones were only or mainly representative of a single fiber population.

3.3. Functionnectome estimation

An example of the estimated 4D functionnectomes and processed Z-statistics activation maps are reported in Supplementary Fig. S4. In general, we observed that, while the standardized functionnectomes covered the entire MNI brain mask, the individualized ones were more consistent with the subject-specific anatomy. Additionally, while CSD-based functionnectomes appeared qualitatively similar, the tensor-based one had strong and unplausible intensity gradients in neighbouring voxels. Moreover, the PFT-based functionnectomes covered larger portions of the grey matter compared to the iFOD2-based one, confirming that the first method provides anatomical priors extending deeper into the grey matter.

3.4. Experiments

3.4.1. Reliability of the priors

Examples of the corresponding tractogram and functionnectome components for the main brain circuits in a single subject are reported in Fig. 2. To show the comparison among the three individualized approaches, the same subject was selected for each approach, especially based on the TensorDet result, which had significantly lower spatial extension and was visually harder to identify with respect to the others; therefore, note that the result shown was not the best one achieved for each modality. The average Pearson's correlation across subjects (mean ± standard deviation) between the tractogram and the functionnectome independent components for the motor, language, control, visual and default mode circuits is reported in Table 1. The statistical analysis demonstrated a significant difference in the results between the probabilistic and the deterministic methods for each of the circuits evaluated ($p < 0.05$). Based on these results, the TensorDet-based method was discarded for the following steps. Additionally, the correlation was

Table 1
Pearson's correlation between the tractogram and the functionnectome independent components for the motor, language, control, visual and default mode circuits. * = adjusted $p < 0.05$; ** = adjusted $p < 0.01$; *** = adjusted $p < 0.001$; **** = adjusted $p < 0.0001$.

	Motor	Language	Control	Visual	DMN
PFT	0.51±0.07	0.48±0.15	0.50±0.11	0.51±0.10	0.38±0.09
iFOD2	0.52±0.09	0.49±0.18	0.58±0.05	0.38±0.10	0.32±0.05
TensorDet	0.24±0.09	0.18±0.06	0.22±0.07	0.35±0.10	0.20±0.07

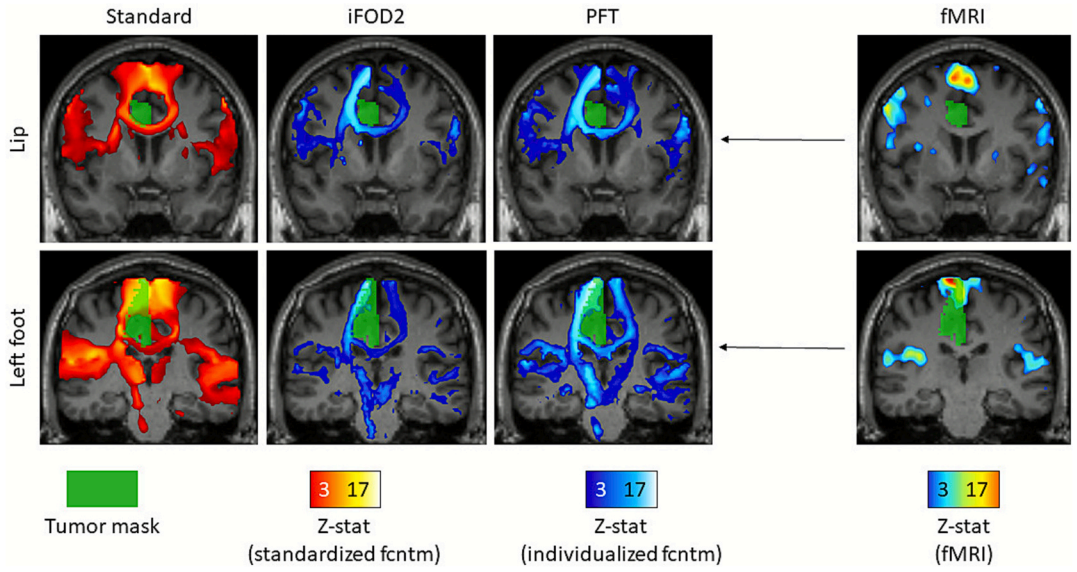

Fig. 3. Functionnectome activation maps for two motor tasks, lip protrusion and left foot plantar flexion. The two individualized cases, which have a good overlap, when compared to the standardized one, appear to be more selective of involved regions and to have a higher statistical activation in correspondence of the motor corpus callosum for lip protrusion and the right cortico-spinal tract for the left foot plantar flexion. The fMRI Z-statistic map for both motor tasks is also shown on the right side of the image. fcntm = functionnectome.

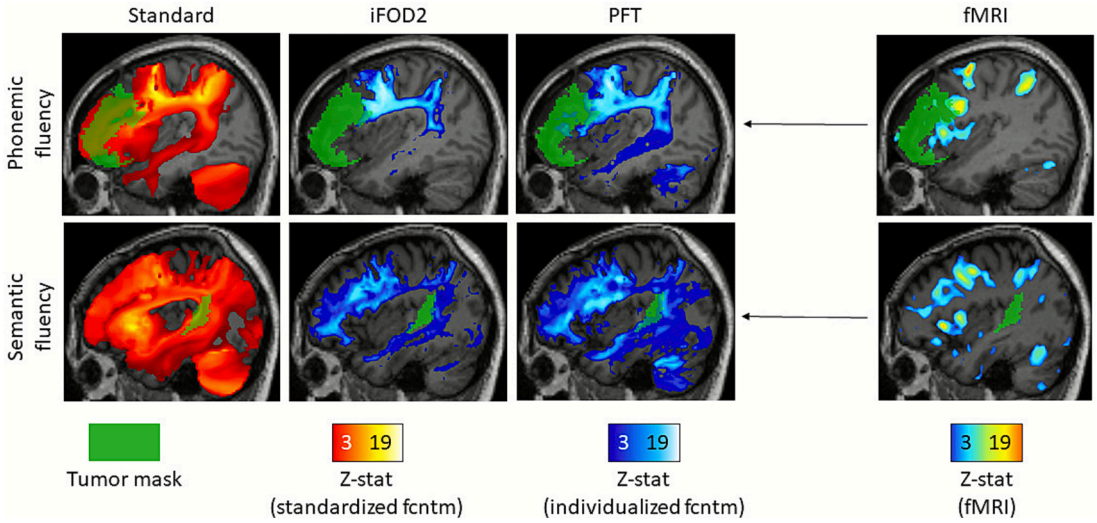

Fig. 4. Functionnectome activation maps for two language tasks, phonemic and semantic fluency. The two individualized cases, when compared to the standardized one, appear to be more selective of the involved white matter circuits and they have a much lower overlap with the tumor. The fMRI Z-statistic map for both language tasks is also shown on the right side of the image. fcntm = functionnectome.

significantly higher for PFT compared to iFOD2 for the control and visual circuits ($p < 0.05$). The correlation values ~ 0.5 for most of the evaluated circuits using PFT and iFOD2 indicated that about 25 % of the variance of the functionnectome component was explained by the

corresponding tractogram component.

3.4.2. Similarity metrics between functionnectomes

Results of the activation maps of the functionnectomes derived in the individualized and standardized cases are shown in Fig. 3 for two cases of motor task and in Fig. 4 for two cases of language tasks. In both cases, the individualized maps overlapped well with each other, with the PFT approach covering a slightly larger area than iFOD2, which is even more evident in the language case. Compared to the standardized maps, the individualized ones, while preserving a similar structure, do not extend as much. While the overlap with tumor is small both in the standardized and individualized functionnectomes for motor tasks, it is significantly higher for language tasks using the standardized method.

The average result (mean ± standard deviation) across subjects of the similarity metrics is reported in Table 2 for the motor tasks and Table 3 for the language tasks. Considering the motor tasks, the Pearson's correlation was significantly lower ($p < 0.01$) between the standardized approach and both the individualized ones (0.57 ± 0.12 for standardized-PFT, 0.51 ± 0.10 for standardized-iFOD2), compared to the correlation between the PFT and the iFOD2 (0.75 ± 0.06). An analogous result was found for language tasks, where also a lower correspondence emerged between standardized and iFOD2 (0.45 ± 0.09), compared to standardized and PFT (0.55 ± 0.07). For both motor and language tasks, the Dice coefficient showed similar values when comparing standardized with PFT (0.57 ± 0.08) and PFT with iFOD2 (0.58 ± 0.05) functionnectomes, while they were significantly higher than the ones obtained comparing standardized with iFOD2 (0.38 ± 0.07) functionnectomes. Together, these results suggest that there is a greater overlap in terms of the extension of the activation maps between the standardized and individualized PFT approaches. However, the higher Pearson's correlation between the two individualized methods indicates that the individual characteristics, which can only be accounted for by the individualized approaches, retain a high relevance. The standardized activation maps had overall a greater overlap with tumor compared to the individualized ones. The difference between the methodologies was significant for language tasks ($p < 0.01$): while the standardized case exhibited a percent overlap of 58 ± 30 %, the PFT had 8 ± 13 %, and iFOD2 2 ± 3.

Given the higher overlap and correlation between the standardized and the PFT approaches, compared to iFOD2, the PFT individualized functionnectomes were selected for the following step.

3.4.3. Functionnectome overlap with tract atlas

For motor tasks, the individualized functionnectome achieved higher consistency in identifying the most plausible motor tracts (such as the cortico-spinal tract and the motor corpus callosum), compared to the standardized functionnectome, which instead showed typically lower values and maximum for cerebellar tracts. In particular, for the right finger tapping (N = 13 patients), at $Z > 3$ the PFT functionnectomes mostly overlapped the left dentato-rubro-thalamic tract (77 % of the cases), cortico-spinal tract (69 %) and motor corpus callosum (54 %), while the standardized case had generally lower across-subject agreement and mostly overlapped the right middle cerebellar peduncle (46 %). Very similarly, for the left finger tapping (N = 13), at $Z > 3$ the PFT functionnectome mostly overlapped the motor corpus callosum (69 %), while the standardized case; with overall lower percentages, had the highest overlap with with the left (46 %) and right (53 %) inferior cerebellar peduncles. In the case of the right foot plantar flexion (N = 5) task, at $Z > 3$ the PFT functionnectome achieved the highest across-subject overlap for the the left cortico-spinal tract, medial lemniscus, parietal thalamic radiation and middle cerebellar peduncle (60 %), while the standardized case reached the highest percentages for the left middle and inferior cerebellar peduncles (60 %). Similarly, for the left foot plantar flexion (N = 5) task, at $Z > 3$ the individualized functionnectome had perfect consistency in identifying the right cortico-spinal tract and medial lemniscus (100 %), whereas the standardized case had the best overlap with the right parietal thalamic radiation and medial lemniscus (60 %). For lip protrusion tasks (N = 9), the across-subject consistency of the tract overlap was not as good as in the previous cases, being below 45 % for each tract both in the individualized and standardized scenarios.

Fig. 5 shows the overlap of the functionnectome activation maps at $Z > 3$ for each of the motor tasks, which are shared by at least 50 % of the involved subjects. The visual inspection of these images notably revealed that the shared maps across individualized functionnectomes had a much better integrity along the course of the involved white matter circuits, compared to the standardized case.

Considering language tasks, there was a higher correspondence between shared tracts in the individualized and standardized case, with both approaches exhibiting the highest percentages for the same underlying circuits. In particular, for the phonemic fluency (N = 20), a high consistency in identifying the cerebellar connections (right and left, middle and inferior cerebellar peduncle) was observed (ranging between 50–75 % for PFT functionnectome and 50–70 % for standardized). However, the frontal aslant tract (30 % for both approaches) and the arcuate fasciculus (25 % for PFT, 30 % for standardized) were also identified. Also for the semantic fluency (N = 11) a good correspondence between the PFT and the standardized approaches was observed. However, in this case, the most overlapped tract was the left frontal aslant tract achieving 64 % for PFT functionnectome and 54 % for standardized. Interestingly, at $Z > 7$, the left arcuate fasciculus was the most shared tract using both methods (54 % for PFT, 45 % for standardized), indicating that, even though the activations were diffuse, the most significant ones were located on the main language-associated tract.

The visual inspection of the overlap of the $Z > 3$ Functionnectome activation maps shared by 50 % or more of the subjects for the two language tasks, reported in Fig. 5, demonstrates that both the individualized and standardized approaches well overlap the tracts involved in language circuits, with the individualized one extending less into the recruited regions.

Detailed results for each task are presented in Supplementary Material Part 2 and Supplementary Fig. S5-11.

4. Discussion

In this work, we proposed a new approach to leverage individual structural connectivity within the Functionnectome framework and

Table 2
Mean ± standard deviation across subjects of Pearson's correlation and Dice coefficient between functionnectome activation maps obtained using PFT, iFOD2 and standardized priors for motor tasks. * = adjusted-p < 0.05; ** = adjusted-p < 0.01; *** = adjusted-p < 0.001; **** = adjusted-p < 0.0001.

Motor	Pearson's R		Dice	
Standard-PFT	0.57±0.12	**	0.57±0.08	****
Standard-iFOD2	0.51±0.10	****	0.38±0.07	****
PFT-iFOD2	0.75±0.06		0.58±0.05	

Table 3
Mean ± standard deviation across subjects of Pearson's correlation and Dice coefficient between functionnectome activation maps obtained using PFT, iFOD2 and standardized priors for language tasks. * = adjusted-p < 0.05; ** = adjusted-p < 0.01; *** = adjusted-p < 0.001; **** = adjusted-p < 0.0001.

Language	Pearson's R	Dice
Standard-PFT	0.55±0.07	0.69±0.13
Standard-iFOD2	0.45±0.09	0.49±0.14
PFT-iFOD2	0.67±0.08	0.65±0.10

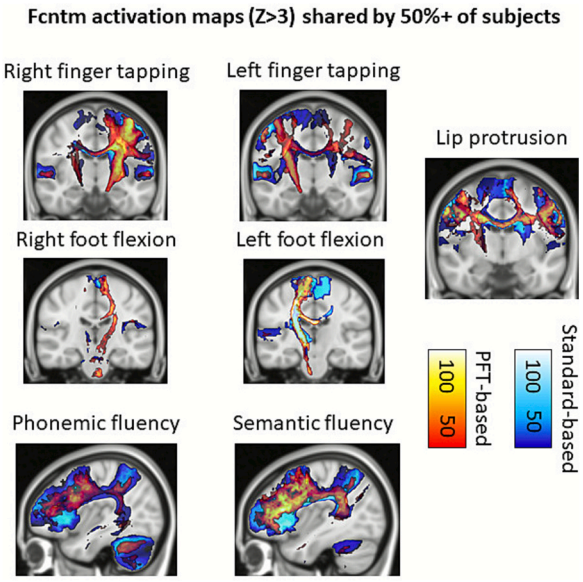

Fig. 5. Percentage of subjects sharing the same voxel in Z > 3 activation maps of PFT (individualized) and standardized functionnectomes for each available motor (top) and language (bottom) task. For motor tasks, it is evident that the individualized approach more robustly reproduced motor pathways in their full course across subjects, compared to the standardized one. In the case of language tasks, the two functionnectome approaches are evidently more overlapped.

evaluated it in patients with brain glioma. By redefining the generation of anatomical priors with probabilistic tractography, we accounted for inter-individual variability and anatomical variability while maintaining compatibility with the original framework. The resulting individualized functionnectomes were reliably constructed and partially overlapped with their standardized counterparts, with stronger agreement when derived using the PFT method, which we selected for further evaluation. Importantly, the individualized approach showed higher consistency in recovering plausible tracts associated with motor activations, and achieved comparable performance to the standardized approach for language tasks, supporting its applicability for subject-specific analyses.

This approach is completely data-driven and it is generally applicable without any assumption on the underlying data. The process to create the individualized anatomical prior was based on an approach similar to that presented by Nozais and colleagues in the latest update of the Functionnectome (Nozais et al., 2023), i.e., starting from a whole-brain tractogram. The key difference lies in the conversion of the tractogram to the set of anatomical priors: while in the original work they are the result of an average of the connectivity across a group of 100 healthy controls, here they were generated at the single subject level, preserving the connections reconstructed in the individual's specific tractogram and weighted to build a probability map based on their anatomical plausibility (Smith et al., 2015).

The need for an individualized translation of the existing group level-derived method was motivated by the fact that the anatomical structure of the brain can be severely disrupted in cases of expansive brain lesions, so that the structural connectivity extrapolated from healthy controls cannot be reliably applied. Additionally, recent evidences suggest that long-range alterations on the brain structural connectivity may emerge in the presence of glioblastoma (Salvalaggio et al., 2024). This view is consistent with a broader movement in the field toward individualized approaches for the study of neurological diseases, in line with the goals of precision medicine for diagnostic and therapeutic purposes (Bansal et al., 2018; Ibrahim et al., 2021; Sighinolfi et al., 2022). Within this context, our results show that individualized priors lead to meaningful differences in the functional involvement of white matter tracts compared to standardized priors. Although the absence of a definitive ground truth complicates validation, the observed spatial distribution of WM activations more closely matched the tracts expected to underlie specific functions, with a higher specificity to each patient's anatomy.

Our results showed that individualized functionnectomes exhibited a more plausible overlap with typically expected white matter bundles across subjects compared to the standardized version. The advantage was particularly clear for motor tasks: individualized functionnectomes consistently identified the relevant motor tracts, reaching 100 % overlap for the left foot plantar flexion, whereas the standardized approach mainly involved cerebellar pathways and at lower frequencies. This indicates that, given the same input spatial distribution of functional activation, the clusters were localized in grey matter regions that were indeed linked by the plausible WM pathways based on the subject-specific structural connectivity, yet following a path with low probability based on the average connectivity of the normative group of healthy controls. The difference persisted at higher Z thresholds, where individualized functionnectomes maintained strong involvement of motor tracts, a result not reproduced by the standardized method. The difference between the two approaches was lower for language tasks, mainly showing the involvement of cerebellar pathways in both cases. On one side, this may be due to the fact that the cerebellar pathways, being uninvolved by the tumor mass, are better reproducible across subjects; on the other side, since the language function is more complex and functionally involves several different brain regions, the projection of the BOLD signal onto the white matter corresponds to a widespread activation of pathways, which does not allow us to properly differentiate the most relevant ones at low Z thresholds. However, the most important language tract, the arcuate fasciculus, was the most consistently identified at higher Z thresholds, suggesting that it still had the greatest statistical involvement. Together, these results suggest that, at least for selective functions, the individualized approaches retain a higher accuracy and specificity than the standardized method, which can be especially relevant in cases of disrupted anatomy and connectivity.

Among the three attempted tractography approaches, the two CSD-based probabilistic ones performed similarly in terms of reliability of the priors, while the deterministic tensor-based approach achieved poorer results. Firstly, this might be explained by the relatively low number of streamlines selected for a whole-brain deterministic tractogram; however, a larger number of streamlines would have significantly increased the computational time of the tractogram-to-connectome

conversion, which is done streamline-wise and takes about 60 min for 1 million tracks. As a consequence, the time required to convert at least 10 times more streamlines would make the performance not comparable with the other two methods. Another reason for the poorer reconstruction may be that, due to the nature of the tensor-based model, the potential range of paths between voxels might be reduced, compared to the diversity that is ensured by drawing the direction from the orientation distribution function (Farquharson et al., 2013; Radwan et al., 2022; Tallus et al., 2023). Both the probabilistic approaches achieved a correlation between the tractogram and the corresponding functionnectome components around 0.5 for the main brain circuits, which corresponds to an explained variance of about 25 %. Therefore, the tractogram explains only a relatively small portion of the variance in functionnectome, even when generated with the individual tractography of the patient, implying that the greatest part of the information is given by the BOLD signal of the grey matter voxels, rather than the pathways over which it is projected. The correlation values we observed are considerably higher than those reported by O'Muircheartaigh & Jbabdi (O'Muircheartaigh and Jbabdi, 2018), which is consistent with the methodological differences between the two approaches. Specifically, their correlations were computed between tractogram and resting-state independent components, whose spatial distributions overlap only modestly because resting-state fMRI activity primarily reflects grey-matter signals, whereas tractography reflects white-matter organization. In our analysis, correlations were instead computed with Functionnectome components, which, by construction, are mostly localized within the white matter—hence a greater anatomical correspondence and higher correlation values. Accordingly, the threshold for significance was 0.22 (≈5% variance explained) in the original approach, compared to the 25 % variance explained in our Functionnectome-based results.The observed correlation values are much higher than those from the original work (O'Muircheartaigh and Jbabdi, 2018), compatibly with the fact that resting-state fMRI ICs clearly have a lower overlap with the tractogram ICs, compared to the Functionnectome ones. Accordingly, the significance of the correlation between the tractogram and the resting-state components was set at 0.22, corresponding to 5 % of the variance explained, compared to the 25 % we found using the Functionnectome.

The agreement between the standardized and the individualized functionnectomes was relatively good for both the cases of the PFT and the iFOD2. As expected, there was not a perfect overlap, since the core idea behind this work was to adhere to the individual subject's idiosyncrasy of the connectivity, and avoid to use the average connectivity of multiple normal controls. However, by achieving a correlation around 0.5, it was demonstrated that the individualized approach, with the redefinition of the probability maps, qualitatively maintained the same structure and basic information as the original, standardized one, projecting the functional data on similar pathways and with comparable statistical values. The correlation, and even more so the Dice coefficient, between the PFT and the standardized functionnectomes was higher than the one between the iFOD2 and the standardized ones. While this result is reasonable considering that the PFT functionnectomes were based on the same tractography method used to generate the standardized priors (Nozais et al., 2023), this may also be partly due to the fact that the PFT, by the nature of the algorithm (Girard et al., 2014), tends to extend streamlines deeper into the grey matter, thus producing larger volumes of significantly activated regions when the fMRI signal is projected onto the white matter and the standardized functionnectomes cover the entire MNI brain volume by definition. However, it is also relevant to note that Pearson's correlation was the highest between the two individualized approaches, compared to their correlations with the standardized functionnectomes. This suggests that the individual variability, which is accounted for by both the individualized functionnectomes, has a greater relevance to the final output than the tractography method itself. The lower overlap with tumor of the individualized approaches with respect to the standardized ones was expected by definition of the anatomical priors, as streamlines could not cross regions where the FOD amplitude was below threshold, which is very likely the case of tumor areas, at least in their core.

The main limitation of the proposed method is the absence of a ground truth to compare it with. However, we proposed three evaluation approaches, to demonstrate its stability and potential: the reliability of anatomical priors, to ensure a good basis for the development of the method; the similarity with the standardized approach, which represents the reference for the novel approach; the analysis of plausibility and consistency, which demonstrate the superior results of the new approach.

Another general limitation is the heterogeneity of the clinical condition of our cohort. Since a specific tumor type was not selected as an inclusion criterion in this study, we cannot make generalized clinical inference on the information that the individualized Functionnectome may provide on the pathology. Moreover, in general, we cannot exclude the possibility that specific tumor types may be more suitable for the individualized evaluation than others, for which a standardized framework would be sufficient, thus inflating our results. Analogously, we did not perform a search of the optimal tractography parameters in the tumoral cases, as this was outside the scope of this work, thus we cannot exclude that it would be possible to achieve equal or better results after parameter tuning. However, there is extensive evidence that advanced tractography methods, including CSD-based ones, can achieve accurate tract reconstruction, with improved sensitivity to peritumoral edema (Yeh et al., 2021). The final CSD-based tractography approach (PFT) selected from this study, which demonstrated better performance than the original method, is the same as the one used to generate standardized priors (Nozais et al., 2023), suggesting that the improvement is related to the individual-specific reconstruction, rather than the tractography method itself. On the other hand, this also shows that the methodological approach we proposed can be reliably applied to different type of brain tumors. Indeed, in principle, the individualized Functionnectome is applicable to any condition, including healthy controls, even if its core potential is more readily evident in cases of altered morphology.

The individualized Functionnectome mostly suffers from the same limitations as whole-brain tractography (Jeurissen et al., 2017), especially the presence of false positives and the overrepresentation of the most straightforward pathways; however, these aspects are mitigated, on one side, by the fact that the final output map of this analysis consists of a statistical assessment of the functionnectome data, so that potential false positive will not have a high impact on the result if they are sparse, and, on the other side, by the streamline weighting provided by SIFT2. Additionally, the same limitations of fMRI, including the low SNR and the sequence duration and temporal resolution, apply to the Functionnectome as well. Longer fMRI acquisitions would most likely produce more selective results.

As much as the limitations of the underlying dMRI and fMRI techniques apply to the Functionnectome, the advantages are inherited as well. From the perspective of fMRI, this implies for example that the analytical techniques developed for functional data, such as effective connectivity, dynamic connectivity and pattern analysis could be applied to the Functionnectome as well, supporting the great potential of this novel technique. The main open question that adopting this procedure arises is whether using the individualized approach, which has a higher computational cost, can provide outcomes with a higher clinical significance compared to the standardized one. This could not be tested in this work, as clinical scales to quantify the patient's condition were not available. However, to correlate or test the capability of clinical outcome prediction of the functionnectome outputs would be a next crucial step. Another future direction would be to compare the individualized and standardized results in healthy controls as well: this would provide additional insights to find whether the improved outcomes that emerged in the presented sample are mostly related to the technique itself or to the unique anatomy that characterizes patients

with expansive lesions. Lastly, this personalized method, if validated, could have a relevant role in the presurgical planning of glioma patients: it would provide a unique information of the statistical involvement of the white matter pathways in key functions that must preserved at resection.

5. Conclusions

We presented a new approach to integrate functional and diffusion MRI data into a single output, based on the conversion of an existing method, the Functionnectome, from a group level-based to a fully individual-dependent framework. We proposed a different approach to achieve an analogous outcome using individualized probability maps of connectivity derived from the subject-specific tractography. The results showed that Functionnectome activation maps retrieved using probabilistic tractography-based priors can achieve a good across-subject reproducibility, improving the standardized method, and a more anatomically plausible overlap with the underlying tracts of known associated functions. This demonstrates the feasibility and the potential relevance even in clinical applications of the use of the individualized approach to estimate functionnectomes, and, on a broader view, it represents a step forward towards personalized medicine.

Data availability statement

The code to generate the individualized anatomical priors will be made available on Zenodo at https://doi.org/10.5281/zenodo.17526354, upon request to the corresponding author, after the publication of the manuscript.

CRediT authorship contribution statement

Giovanni Sighinolfi: Writing – review & editing, Writing – original draft, Validation, Methodology, Formal analysis, Data curation, Conceptualization. **Alexander Leemans:** Writing – review & editing, Supervision, Resources, Project administration, Methodology, Conceptualization. **David Neil Manners:** Writing – review & editing, Supervision, Methodology. **Elena Cantoni:** Writing – review & editing, Data curation. **Gianfranco Vornetti:** Writing – review & editing, Data curation. **Lorenzo Motta:** Writing – review & editing, Data curation. **Enrico Franceschi:** Writing – review & editing, Data curation. **Caterina Tonon:** Writing – review & editing, Supervision, Resources, Project administration, Funding acquisition, Data curation. **Raffaele Lodi:** Writing – review & editing, Supervision, Resources, Project administration, Funding acquisition, Data curation. **Alberto De Luca:** Writing – review & editing, Supervision, Resources, Project administration, Methodology, Conceptualization.

Acknowledgements

The publication of this article was supported by the "Ricerca Corrente" funding from the Italian Ministry of Health.

This work was supported by #NEXTGENERATIONEU (NGEU) and funded by the Ministry of University and Research (MUR), National Recovery and Resilience Plan (NRRP), project MNESYS (PE0000006)—A multiscale integrated approach to the study of the nervous system in health and disease (DN. 1553 11.10.2022).

Declaration of generative AI and AI-assisted technologies in the manuscript preparation process.

During the preparation of this work the authors used ChatGPT in order to improve English writing and phrasing. After using this tool/service, the authors reviewed and edited the content as needed and take full responsibility for the content of the published article.

Appendix A. Supplementary data

Supplementary data to this article can be found online at https://doi.org/10.1016/j.nicl.2025.103940.

Data availability

The code to generate the individualized anatomical priors will be made available on Zenodo at 10.5281/zenodo.17526354, upon request to the corresponding author, after the publication of the manuscript

References

Alstott, J., Breakspear, M., Hagmann, P., Cammoun, L., Sporns, O., 2009. Modeling the Impact of Lesions in the Human Brain. PLoS Comput. Biol. 5, e1000408. https://doi.org/10.1371/journal.pcbi.1000408.

Andersson, J.L., Sotiropoulos, S.N., 2016. An integrated approach to correction for off-resonance effects and subject movement in diffusion MR imaging. Neuroimage 125, 1063–1078. https://doi.org/10.1016/j.neuroimage.2015.10.019.

Andersson, J.L.R., Skare, S., Ashburner, J., 2003. How to correct susceptibility distortions in spin-echo echo-planar images: application to diffusion tensor imaging. Neuroimage 20, 870–888. https://doi.org/10.1016/S1053-8119(03)00336-7.

Bansal, K., Nakuci, J., Muldoon, S., 2018. Personalized brain network models for assessing structure-function relationships. Curr. Opin. Neurobiol. 52, 42–47. https://doi.org/10.1016/j.conb.2018.04.014.

Basser, P.J., Pajevic, S., Pierpaoli, C., Duda, J., Aldroubi, A., 2000. In vivo fiber tractography using DT-MRI data. Magn. Reson. Med. 44, 625–632. https://doi.org/10.1002/1522-2594(200010)44:4%253C625::aid-mrm17%253E3.0.co;2-o.

Brett, M., Markiewicz, C.J., Hanke, M., Côté, M.-A., Cipollini, B., McCarthy, P., Jarecka, D., Cheng, C.P., Halchenko, Y.O., Cottaar, M., Larson, E., Ghosh, S., Wassermann, D., Gerhard, S., Lee, G.R., Baratz, Z., Wang, H.-T., Kastman, E., Kaczmarzyk, J., Guidotti, R., Daniel, J., Duek, O., Rokem, A., Madison, C., Papadopoulos Orfanos, D., Sólon, A., Moloney, B., Morency, F.C., Goncalves, M., Markello, R., Riddell, C., Burns, C., Millman, J., Gramfort, A., Leppäkangas, J., van den Bosch, J.J.F., Vincent, R.D., Braun, H., Subramaniam, K., Van, A., Gorgolewski, K.J., Raamana, P.R., Klug, J., Nichols, B.N., Baker, E.M., Hayashi, S., Pinsard, B., Haselgrove, C., Hymers, M., Esteban, O., Koudoro, S., Pérez-García, F., Dockès, J., Oosterhof, N.N., Amirbekian, B., Christian, H., Nimmo-Smith, I., Nguyen, L., Reddigari, S., St-Jean, S., Panfilov, E., Garyfallidis, E., Varoquaux, G., Legarreta, J.H., Hahn, K.S., Waller, L., Hinds, O.P., Fauber, B., Perez, F., Roberts, J., Poline, J.-B., Stutters, J., Jordan, K., Cieslak, M., Moreno, M.E., Hrnčiar, T., Haenel, V., Schwartz, Y., Darwin, B.C., Thirion, B., Gauthier, C., Solovey, I., Gonzalez, I., Palasubramaniam, J., Lecher, J., Leinweber, K., Raktivan, K., Calábková, M., Fischer, P., Gervais, P., Gadde, S., Ballinger, T., Roos, T., Reddam, V.R., freec84, 2023. nipy/nibabel: 5.1.0. doi:10.5281/zenodo.7795644.

Calamante, F., Masterton, R.A.J., Tournier, J.-D., Smith, R.E., Willats, L., Raffelt, D., Connelly, A., 2013. Track-weighted functional connectivity (TW-FC): a tool for characterizing the structural-functional connections in the brain. Neuroimage 70, 199–210. https://doi.org/10.1016/j.neuroimage.2012.12.054.

Castellano, A., Cirillo, S., Bello, L., Riva, M., Falini, A., 2017. Functional MRI for Surgery of Gliomas. Curr. Treat. Options. Neurol. 19, 34. https://doi.org/10.1007/s11940-017-0469-y.

Castellaro, M., Moretto, M., Baro, V., Brigadoi, S., Zanoletti, E., Anglani, M., Denaro, L., Dell'Acqua, R., Landi, A., Causin, F., d'Avella, D., Bertoldo, A., 2020. Multishell Diffusion MRI-Based Tractography of the Facial Nerve in Vestibular Schwannoma. AJNR Am. J. Neuroradiol. 41, 1480–1486. https://doi.org/10.3174/ajnr.A6706.

Chen, J.E., Glover, G.H., 2015. Functional magnetic Resonance Imaging Methods. Neuropsychol. Rev. 25, 289–313. https://doi.org/10.1007/s11065-015-9294-9.

Cox, R.W., 1996. AFNI: Software for Analysis and Visualization of Functional magnetic Resonance Neuroimages. Comput. Biomed. Res. 29, 162–173. https://doi.org/10.1006/cbmr.1996.0014.

Descoteaux, M., Angelino, E., Fitzgibbons, S., Deriche, R., 2007. Regularized, fast, and robust analytical Q-ball imaging. Magn. Reson. Med. 58, 497–510. https://doi.org/10.1002/mrm.21277.

Dhollander, T., Mito, R., Raffelt, D., Connelly, A., 2019. Improved white matter response function estimation for 3-tissue constrained spherical deconvolution. Presented at the ISMRM 27th Annual Meeting & Exhibition.

Dhollander, T., Raffelt, D., Connelly, A., 2016. Unsupervised 3-tissue response function estimation from single-shell or multi-shell diffusion MR data without a co-registered T1 image, in: ISMRM Workshop on Breaking the Barriers of Diffusion MRI. p. 5.

Farquharson, S., Tournier, J., Calamante, F., Fabinyi, G., Schneider-Kolsky, M., Jackson, G., Connelly, A., 2013. White matter fiber tractography: why we need to move beyond DTI. J. Neurosurg. 118, 1367–1377. https://doi.org/10.3171/2013.2.JNS121294.

Fornito, A., Zalesky, A., Breakspear, M., 2015. The connectomics of brain disorders. Nat. Rev. Neurosci. 16, 159–172. https://doi.org/10.1038/nrn3901.

Foulon, C., Cerliani, L., Kinkingnéhun, S., Levy, R., Rosso, C., Urbanski, M., Volle, E., Thiebaut de Schotten, M., 2018. Advanced lesion symptom mapping analyses and implementation as BCBtoolkit. GigaScience 7, 1–17. https://doi.org/10.1093/gigascience/giy004.

Girard, G., Whittingstall, K., Deriche, R., Descoteaux, M., 2014. Towards quantitative connectivity analysis: reducing tractography biases. Neuroimage 98, 266–278. https://doi.org/10.1016/j.neuroimage.2014.04.074.

Harris, C.R., Millman, K.J., van der Walt, S.J., Gommers, R., Virtanen, P., Cournapeau, D., Wieser, E., Taylor, J., Berg, S., Smith, N.J., Kern, R., Picus, M., Hoyer, S., van Kerkwijk, M.H., Brett, M., Haldane, A., del Río, J.F., Wiebe, M., Peterson, P., Gérard-Marchant, P., Sheppard, K., Reddy, T., Weckesser, W., Abbasi, H., Gohlke, C., Oliphant, T.E., 2020. Array programming with NumPy. Nature 585, 357–362. https://doi.org/10.1038/s41586-020-2649-2.

Ibrahim, A., Primakov, S., Beuque, M., Woodruff, H., Halilaj, I., Wu, G., Refaee, T., Granzier, R., Widaatalla, Y., Hustinx, R., Mottaghy, F., Lambin, P., 2021. Radiomics for precision medicine: current challenges, future prospects, and the proposal of a new framework. Methods 188, 20–29. https://doi.org/10.1016/j.ymeth.2020.05.022.

Jenkinson, M., Bannister, P., Brady, M., Smith, S., 2002. Improved optimization for the robust and accurate linear registration and motion correction of brain images. Neuroimage 17, 825–841. https://doi.org/10.1006/nimg.2002.1132.

Jenkinson, M., Beckmann, C.F., Behrens, T.E.J., Woolrich, M.W., Smith, S.M., 2012. FSL. Neuroimage 62, 782–790.

Jeurissen, B., Descoteaux, M., Mori, S., Leemans, A., 2017. Diffusion MRI fiber tractography of the brain. NMR Biomed. 32. https://doi.org/10.1002/nbm.3785.

Jeurissen, B., Tournier, J.-D., Dhollander, T., Connelly, A., Sijbers, J., 2014. Multi-tissue constrained spherical deconvolution for improved analysis of multi-shell diffusion MRI data. Neuroimage 103, 411–426. https://doi.org/10.1016/j.neuroimage.2014.07.061.

Lakhani, D.A., Sabsevitz, D.S., Chaichana, K.L., Quiñones-Hinojosa, A., Middlebrooks, E. H., 2023. Current State of Functional MRI in the Presurgical Planning of Brain Tumors. Radiol. Imaging Cancer 5, e230078. https://doi.org/10.1148/rycan.230078.

Liégeois, R., Santos, A., Matta, V., Van De Ville, D., Sayed, A.H., 2020. Revisiting correlation-based functional connectivity and its relationship with structural connectivity. Network Neurosci. 4, 1–25. https://doi.org/10.1162/netn_a_00166.

Logothetis, N.K., 2003. The underpinnings of the BOLD functional magnetic resonance imaging signal. J. Neurosci. 23, 3963–3971. https://doi.org/10.1523/JNEUROSCI.23-10-03963.2003.

Mandke, K., Meier, J., Brookes, M.J., et al., 2018. Comparing multilayer brain networks between groups: introducing graph metrics and recommendations. Neuroimage 166, 371–384. https://doi.org/10.1016/j.neuroimage.2017.11.016.

Manners, D.N., Gramegna, L.L., La Morgia, C., Sighinolfi, G., Fiscone, C., Carbonelli, M., Romagnoli, M., Carelli, V., Tonon, C., Lodi, R., 2022. Multishell Diffusion MR Tractography yields Morphological and Microstructural Information of the Anterior Optic Pathway: a Proof-of-Concept Study in patients with Leber's Hereditary Optic Neuropathy. Int. J. Environ. Res. Public Health 19, 6914. https://doi.org/10.3390/ijerph19116914.

Muccioli, L., Sighinolfi, G., Mitolo, M., Ferri, L., Rochat, M.J., Pensato, U., Taruffi, L., Testa, C., Masullo, M., Cortelli, P., et al., 2023. Cognitive and functional connectivity impairment in post-COVID-19 olfactory dysfunction. NeuroImage: Clinical 38, 103410. https://doi.org/10.1016/j.nicl.2023.103410.

Nozais, V., Forkel, S.J., Foulon, C., Petit, L., Thiebaut de Schotten, M., 2021. Functionnectome as a framework to analyse the contribution of brain circuits to fMRI. Commun. Biol. 4, 1035. https://doi.org/10.1038/s42003-021-02530-2.

Nozais, V., Theaud, G., Descoteaux, M., Thiebaut de Schotten, M., Petit, L., 2023. Improved Functionnectome by dissociating the contributions of white matter fiber classes to functional activation. Brain Struct. Funct. 228, 2165–2177. https://doi.org/10.1007/s00429-023-02714-y.

O'Muircheartaigh, J., Jbabdi, S., 2018. Concurrent white matter bundles and grey matter networks using independent component analysis. Neuroimage 170, 296–306. https://doi.org/10.1016/j.neuroimage.2017.05.012.

Park, H., Friston, K., 2013. Structural and functional brain networks: from connections to cognition. Science 342, 1238411. https://doi.org/10.1126/science.1238411.

Radwan, A.M., Sunaert, S., Schilling, K., Descoteaux, M., Landman, B.A., Vandenbulcke, M., Theys, T., Dupont, P., Emsell, L., 2022. An atlas of white matter anatomy, its variability, and reproducibility based on constrained spherical deconvolution of diffusion MRI. Neuroimage 254, 119029. https://doi.org/10.1016/j.neuroimage.2022.119029.

Ritter, P., Schirner, M., McIntosh, A.R., Jirsa, V.K., 2013. The virtual brain integrates computational modeling and multimodal neuroimaging. Brain Connect. 3, 121–145. https://doi.org/10.1089/brain.2012.0120.

Rojkova, K., Volle, E., Urbanski, M., Humbert, F., Dell'Acqua, F., Thiebaut de Schotten, M., 2016. Atlasing the frontal lobe connections and their variability due to age and education: a spherical deconvolution tractography study. Brain Struct. Funct. 221, 1751–1766. https://doi.org/10.1007/s00429-015-1001-3.

Salvalaggio, A., Pini, L., Bertoldo, A., Corbetta, M., 2024. Glioblastoma and brain connectivity: the need for a paradigm shift. The Lancet Neurology 23, 740–748. https://doi.org/10.1016/S1474-4422(24)00160-1.

Sighinolfi, G., Mitolo, M., Testa, C., Martinoni, M., Evangelisti, S., Rochat, M., Zoli, M., Mazzatenta, D., Lodi, R., Tonon, C., 2022. What can Resting-State fMRI Data Analysis Explain about the Functional Brain Connectivity in Glioma patients? Tomography 8, 267–280. https://doi.org/10.3390/tomography8010021.

Smith, R.E., Tournier, J., Calamante, F., Connelly, A., 2015. SIFT2: Enabling dense quantitative assessment of brain white matter connectivity using streamlines tractography. Neuroimage 119, 338–351. https://doi.org/10.1016/j.neuroimage.2015.06.092.

Smith, R.E., Tournier, J.D., Calamante, F., Connelly, A., 2012. Anatomically-constrained tractography: improved diffusion MRI streamlines tractography through effective use of anatomical information. Neuroimage 62, 1924–1938. https://doi.org/10.1016/j.neuroimage.2012.06.005.

Tallus, J., Mohammadian, M., Kurki, T., Roine, T., Posti, J., Tenovuo, O., 2023. A comparison of diffusion tensor imaging tractography and constrained spherical deconvolution with automatic segmentation in traumatic brain injury. Neuroimage Clin 37, 103284. https://doi.org/10.1016/j.nicl.2022.103284.

Tarun, A., Behjat, H., Bolton, T., Abramian, D., Van De Ville, D., 2020. Structural mediation of human brain activity revealed by white-matter interpolation of fMRI. Neuroimage 213, 116718. https://doi.org/10.1016/j.neuroimage.2020.116718.

Theaud, G., Houde, J.C., Bore, A., Rheault, F., Morency, F., Descoteaux, M., 2020. TractoFlow: a robust, efficient and reproducible diffusion MRI pipeline leveraging Nextflow & Singularity. Neuroimage 218, 116889. https://doi.org/10.1016/j.neuroimage.2020.116889.

Tournier, J.-D., Calamante, F., Connelly, A., 2010. Improved probabilistic streamlines tractography by 2nd order integration over fibre orientation distributions, in: Proc. Intl. Soc. Mag. Reson. Med. p. 1670.

Tournier, J.-D., Smith, R., Raffelt, D., Tabbara, R., Dhollander, T., Pietsch, M., Christiaens, D., Jeurissen, B., Yeh, C.-H., Connelly, A., 2019. MRtrix3: a fast, flexible and open software framework for medical image processing and visualisation. Neuroimage 202, 116137. https://doi.org/10.1016/j.neuroimage.2019.116137.

Van Essen, D.C., Smith, S.M., Barch, D.M., Behrens, T.E., Yacoub, E., Ugurbil, K., Consortium, W.-M., 2013. The WU-Minn human connectome project: an overview. Neuroimage 80, 62–79. https://doi.org/10.1016/j.neuroimage.2013.05.041.

Woolrich, M.W., Ripley, B.D., Brady, M., Smith, S.M., 2001. Temporal Autocorrelation in Univariate Linear Modeling of FMRI Data. Neuroimage 14, 1370–1386. https://doi.org/10.1006/nimg.2001.0931.

Yeh, F.-C., Irimia, A., de Bastos, D.C., A., Golby, A.J., 2021. Tractography methods and findings in brain tumors and traumatic brain injury. Neuroimage 245, 118651. https://doi.org/10.1016/j.neuroimage.2021.118651.

Zhang, Y., Brady, M., Smith, S., 2001. Segmentation of brain MR images through a hidden Markov random field model and the expectation-maximization algorithm. IEEE Trans. Med. Imaging 20, 45–57. https://doi.org/10.1109/42.906424.